ACS APPLIED MATERIALS & INTERFACES

www.acsami.org

Research Article

Reversible Rectification of Microscale Ferroelectric Junctions Employing Liquid Metal Electrodes

Lifa Ni, Xiaojin Li, Zhibin Zhao, Jongwoo Nam, Pengfei Wu, Qingling Wang, Takhee Lee,* Hongliang Liu,* and Dong Xiang*

Cite This: *ACS Appl. Mater. Interfaces* 2021, 13, 29885−29893

Read Online

ACCESS | Metrics & More | Article Recommendations | Supporting Information

ABSTRACT: Both ferroelectric crystals and liquid metal electrodes have attracted extensive attention for potential applications in next-generation devices and circuits. However, the interface information between ferroelectric crystals and liquid metal electrodes has so far been lacking. To better understand the optoelectronic properties of microscale ferroelectric crystals (potassium tantalate niobate, KTN) and its potential integration with liquid metal electrodes (a "printing ink" for flexible electric circuit production), microscale KTN crystals sandwiched by eutectic gallium indium (EGaIn, a liquid metal) with varied contact geometries were studied. Unlike the bulk KTN crystal junctions, the microscale KTN junctions show electrical rectifying characteristics upon light illumination, and the directionality of the rectification can be reversed by increasing the ambient temperature to a few degrees. Furthermore, a strong suppression of the current upon increasing voltage, that is, the quasi-negative differential resistance, is observed when the microscale KTN is half-enclosed by the EGaIn electrode. Our results show that trapping/detrapping of carriers affected by the crystal size and the ambient temperature is the dominant physical mechanism for these observations. These results not only facilitate a better understanding of charge transport through the microscale ferroelectric crystals but also advance the design of miniaturized hybrid devices.

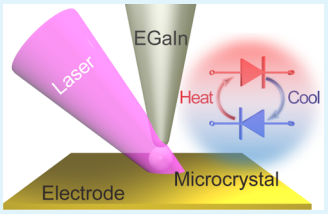

KEYWORDS: *switchable rectification, current suppression, charge trapping and detrapping, potassium tantalate niobate crystal, eutectic gallium indium electrode*

INTRODUCTION

Recently, ferroelectric junctions have attracted intensive attention for potential applications in next-generation memory devices,[1−5] switchable diodes,[6] and electro−optical modulators.[7] Potassium tantalate niobate ($KTa_{1-x}Nb_xO_3$, KTN) crystal as a ferroelectric material has also attracted considerable attention due to its potential applications in functional optoelectronic devices on the basis of its unique characteristics,[8−10] such as giant piezoelectric coefficients,[11,12] large electro-optical effects,[13,14] adjustable polar nanoregions, and the electrocaloric effect.[15] However, the electrical properties of KTN particles upon light illumination have been rarely studied. To better understand the device performance and make the best use of the KTN crystals, it is essential to understand the optoelectrical properties of microcrystals, which may differ from the properties of bulk crystals. So far, it is still a challenge to probe the rigid micro/nanoscale crystals with a stable/tight contact without mechanical damage/scratches to the sample. Scanning tunneling microscopy (STM) is a powerful technique to be employed for probing the electrical properties of microscale/nanoscale crystals, while the sample surface scratching by the rigid STM tip should be carefully avoided.[16] Sputtering or evaporating a metal layer as the top electrode is frequently used for the contact of bulk/film crystals.[17] However, the method of sputtering/evaporating a metal layer is not suitable for microscale crystals (especially for those particles with an irregular shape) because the top and bottom electrodes may be short-circuited during the metal evaporation process.

To address this technical problem, a soft liquid metal (EGaIn) electrode[18−25] was exploited to probe the electrical properties of microscale KTN crystals. The adaptive deformation of the EGaIn electrode makes it feasible to establish a stable/tight electrode/crystal with varied contact geometries without mechanical damage to the samples.[26] By taking the advantages of EGaIn electrodes, the optoelectrical properties of both large and small KTN crystals were studied. Two interesting phenomena, that is, temperature-controlled rectification and contact area-mediated carrier transport in microscale KTN junctions, were reported for the first time.

Rectification with unidirectional electric current flow, that is, one direction current is allowed and the opposite current is suppressed, is an indispensable element in modern electronics.[27−29] Normally, the rectifying direction is fixed as far as the device is fabricated. Lee et al. reported a switchable

Received: December 28, 2020
Accepted: June 9, 2021
Published: June 17, 2021

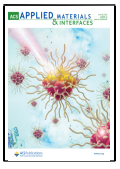

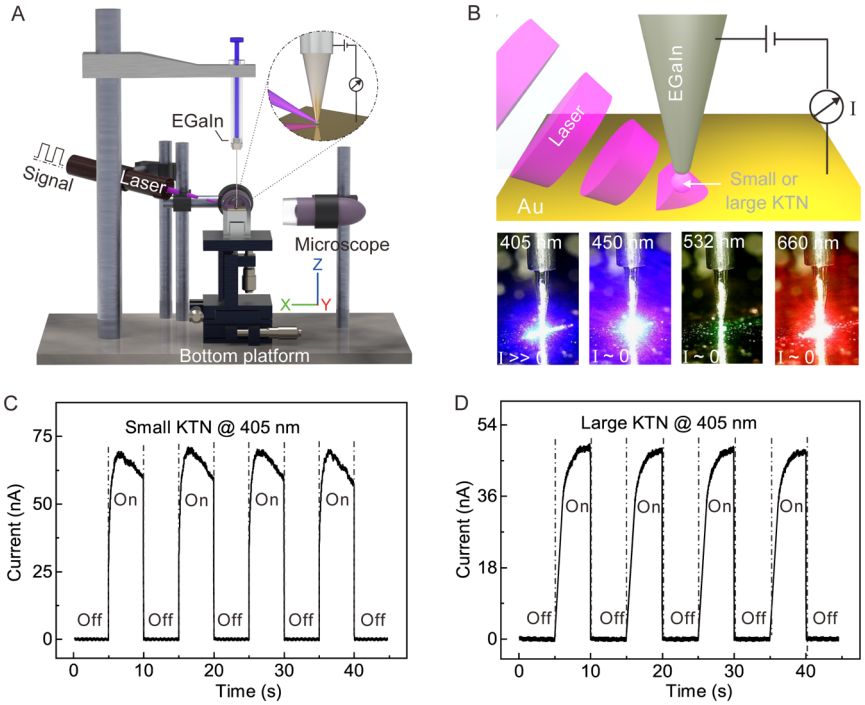

Figure 1. Real-time photocurrent response of KTN junctions. (A) Schematic of the experimental setup. The EGaIn−KTN−Au junction is formed by raising the bottom electrode via piezo control. (B) Electrical measurement of the junctions upon light illumination with a small or a large KTN particle. A considerable current is observed as the junction is illuminated with a purple laser (405 nm). (C) Photocurrent response of small (~50 μm) and (D) large-size (~200 μm) KTN particles upon 405 nm laser (3 mW) illumination under a fixed bias voltage (10 V).

ferroelectric diode in which the directionality of the diode can be reproducibly switched by applying large external electric voltage pulses (poling voltage) to reverse the ferroelectric polarization.[6] Here, we report that the rectification direction of microscale asymmetric EGaIn−KTN−Au junctions can be reversed just by increasing the ambient temperature to a few degrees above the room temperature with a completely different operating mechanism.

The phenomenon of the decrease of current with increasing voltage is known as the negative differential resistance (NDR) effect,[30,31] which has attracted tremendous attention because it is one of the primary elements for nanoelectronic applications in low-power memory devices[32] and logic circuits,[33,34] high-frequency oscillators,[35] and high electron mobility transistors.[36] Here, a quasi-NDR behavior, that is, the current is strongly suppressed but not decreases upon increasing voltage, is observed as the contact area is largely increased by compressing the symmetric EGaIn−KTN−EGaIn junction. It is revealed that the current suppression should mainly originate from the carrier trapping/detrapping processes due to the increase of surface defects by the extended area of the electrode contract. Our study provides a method to mediate the carrier transport through microscale KTN via the control of contact geometries. The two findings and corresponding analysis indicate that the interface between microscale KTN and the electrode plays an important role in determining the performance of the devices, which may help in the fabrication of next-generation memory devices or other vital devices in dealing with the interface issue.

RESULTS AND DISCUSSION

Crystal Size Effect on Photocurrent in KTN Junctions. Figure 1 shows the experimental setup for the junction formation and the electrical measurements under laser illumination. To form an asymmetric EGaIn−KTN−Au junction, a piezo actuator with a nanometer precision is used to control the movement of the bottom gold electrode. The microscale KTN crystal above the bottom electrode is obtained by crushing a bulk KTN crystal (Figure S1). The EGaIn electrode with a conical tip is fixed on the bracket as a top electrode. The fabrication of an EGaIn conical tip covered with a spontaneously formed ultrathin GaO_x layer[37] can be found in Figure S2 and Video S1. The formation of the EGaIn−KTN−Au junction is monitored by two orthogonally aligned microscopes (Figure S3 and Video S2).

To test the photoresponse of microscale KTN, four power-adjustable lasers are used as stimulation sources (Figure S4A,B). No obvious photocurrent is observed when KTN is illuminated by the lasers of 450, 532, and 660 nm. In contrast, a large photocurrent response is observed when the KTN is illuminated by a 405 nm laser and the photocurrent increases linearly with the power of the laser (Figures 1B and S4C). It is reasonable because the purple light (~405 nm) with a higher photon energy (~3.1 eV) has high possibility to excite the electrons from the KTN valence band to the conduction band to generate free carriers.[38] This observation agrees well with the measurements of transmission spectra of KTN. The transmittance is approximately 25% for the 405 nm laser but increases rapidly to a value higher than 65% for the 450 nm laser (Figure S4D).

The photocurrent responses of the KTN particles with two different sizes (~50 and ~200 μm in diameter) are shown in Figure 1C,D, respectively. It can be found that the photocurrent decreases sharply to zero for both sizes of the crystal as the light is turned off. The smaller-sized and larger-sized KTN particles show a significantly different photocurrent response upon light illumination. The photocurrent increases sharply to

https://doi.org/10.1021/acsami.0c22925
ACS Appl. Mater. Interfaces 2021, 13, 29885−29893

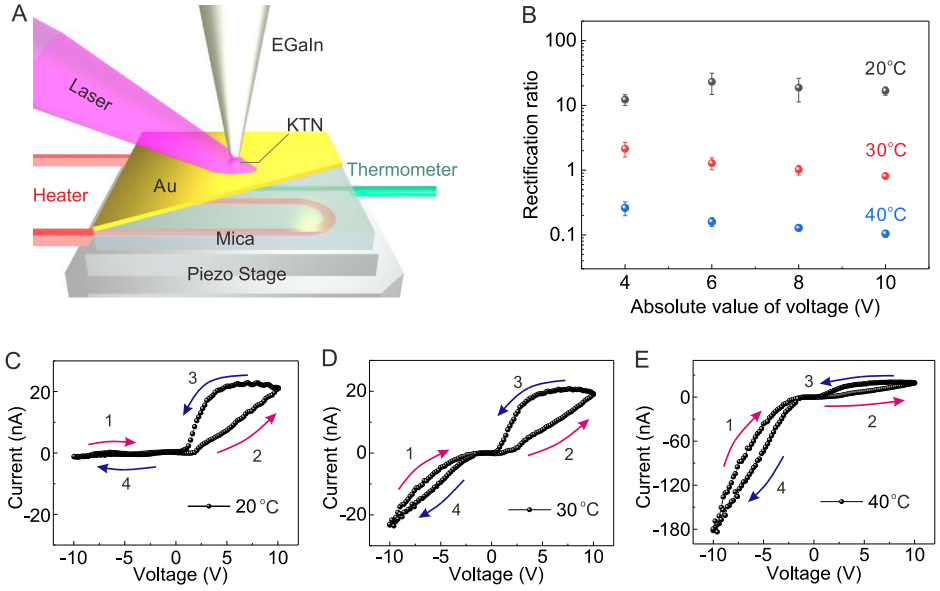

Figure 2. Characterization of photogenerated carrier transport through the EGaIn−KTN−Au junction at different temperatures. (A) Schematic of the temperature controlling system for the junction integrated with a fiber laser illumination system. (B) Rectification ratio of the KTN junction at different temperatures. The error bar is calculated based on five repeated measurements. (C−E) *I*−*V* curves during double voltage sweep measured at 20, 30, and 40 °C, respectively. The numbers show the sequence of the voltage sweep process, the red/blue arrows indicate the forward/backward voltage sweep.

a maximum value followed by a decay upon light illumination for the small-size KTN, as shown in Figure 1C. In contrast, for the large size, KTN the photocurrent increases slowly to a maximum value upon the light illumination, then decreases sharply to zero as the light is turned off, as shown in Figure 1D. We attribute these results to the factor that the applied electric field in small-size KTN is much larger than the one in large-size KTN. Under a large electric field, the photogenerated carriers will be separated more efficiently leading to a fast increase of the current, followed by a decay due to carrier recombination. In contrast, the photogenerated electron−hole pairs cannot be separated efficiently under weak fields in large-size KTN, thus the electrons and holes have high possibility to recombine again, which results in a slow increase of the photocurrent.

Upon the same bias voltage, the current passing the small-size crystal is larger than the one passes the large-size KTN even though the number of photogenerated carriers in large-size KTN is greater than the one in small-size KTN, as presented in Figure 1C,D. We attribute this observation to the facts: (1) the electrical field strength in small-size KTN is larger than the one in large-size KTN as mentioned above. The photogenerated carriers will be separated more efficiently under the larger electric field, which will lead to a larger current for small-size KTN;[39−41] (2) The electron−hole transport length in large KTN is longer than the one in small-size KTN. The long transport length will make the photogenerated carries highly probable to be recombined before they are collected by the electrodes, which may lead to a decrease of the photocurrent.[42,43] A similar experiment is performed, which shows that the current obviously decreases when the thickness of the KTN and the applied voltage are increased by approximately 100% simultaneously to maintain the strength of the electrical field. A further experiment shows that only a negligibly low current (∼0.1 nA @ ±10 V) is observed under light illumination (405 nm, 3 mW) when a bulk KTN crystal is employed with a thickness of 1 mm (Figure S5).

Reversible Rectification Mediated by Ambient Temperature. The electrical measurement system under light illumination combined with a temperature control system is schematically illustrated in Figure 2A. A resistance heating wire is buried under a mica sheet (100 μm in thickness) on which an Au layer is evaporated. The local temperature will increase when a voltage is applied to the resistance wire. The temperature near the junction is measured using a thermometer, and the two-dimensional (2D) temperature distribution around the whole junction is mapped using a thermal infrared imager (Figure S6). All the double sweep current−voltage (*I*−*V*) curves at different temperatures show a hysteresis characteristic, as presented in Figure 2C−E, which can be attributed to the effect of spontaneous polarization of the ferroelectric material.

Instead of hysteresis, we focus on the rectification behavior of the microscale KTN at different temperatures. Here, the rectification ratio is defined as: $R = I_{(+V)}/I_{(-V)}$, where $I_{(+V)}$ is the current under positive bias and $I_{(-V)}$ is the current under counterpart negative bias. It is found that the *R* value varies from ∼20 to ∼0.1 when the temperature increases from 20 to 40 °C under large bias voltage, as summarized in Figure 2B. Notably, the photocurrent is very small and the rectification ratio shows large fluctuation at small bias. Therefore, the rectification ratio at 2 V is not plotted in Figure 2B. At the initial room temperature (20 °C), the overall current at a negative bias is strongly suppressed, which results in that the negative current is much smaller than the positive current ($R \sim 20$), as shown in Figure 2C.

This negative current is strongly enhanced by more than an order of magnitude as the temperature increases from 20 to 30 °C, while the positive current mainly remains unchanged. The *I*−*V* curve is approximately symmetric ($R \sim 1$) at 30 °C, as shown in Figure 2D. The negative current is further enhanced by an order of magnitude as the temperature increases further from 30 to 40 °C, resulting in a reversed rectification ($R \sim 0.1$), as shown in Figure 2E. Such temperature-influenced

https://doi.org/10.1021/acsami.0c22925
ACS Appl. Mater. Interfaces 2021, 13, 29885−29893

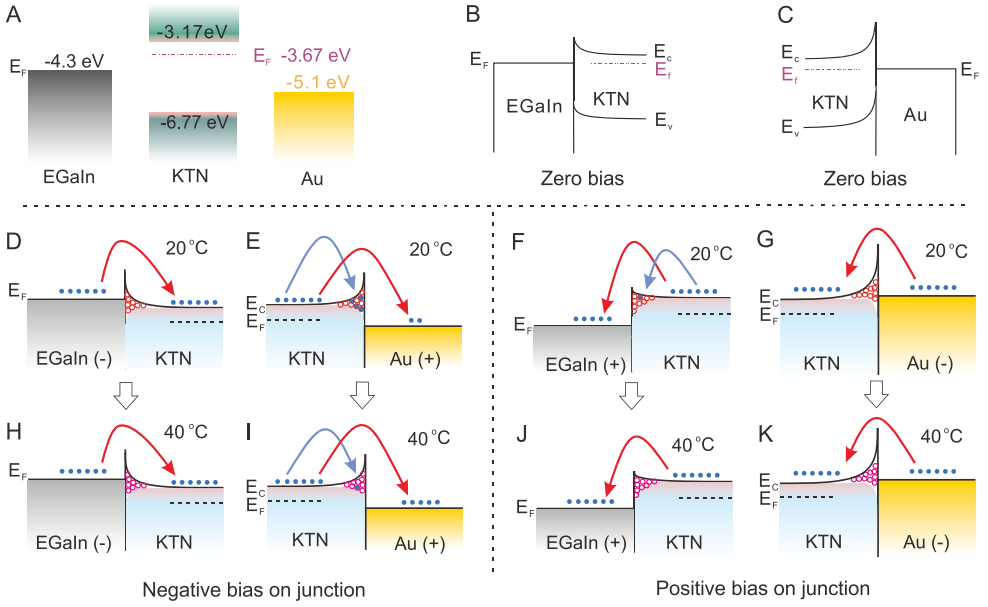

Figure 3. Mechanism for the reversible rectification in the KTN junction mediated by the temperature. (A) Energy band alignment between KTN and two electrodes before contacts. (B,C) Energy landscape of the EGaIn/KTN and KTN/Au interface under zero bias. The electron transfer at the EGaIn/KTN and KTN/Au interfaces at low temperature when a (D,E) negative bias or (F,G) positive bias is applied to the junction. The blue dot/red circle represents the electron/defects. The red arrow shows the electron crossover of the Schottky barrier, and the blue arrow indicates the electron is trapped by the defects. The electron transferring at two interfaces under (H,I) negative bias or under (J,K) positive bias when temperature is increased from 20 to 40 °C.

rectification is observed using different EGaIn−KTN−Au junctions with microscale KTN crystals. It is further found that the influence of temperature on the rectification ratio depends on the crystal size, that is, the rectification ratio for the smaller crystal is more sensitive to the ambient temperature change than the larger one (Figure S7).

The increase of negative current with the increase of temperature is partly attributed to the change of spontaneous polarization.[44] Generally, the polar nanoregions (PNRs)[45] occur at a temperature higher than Curie temperature (T_c), which is determined to be −8 °C for our samples (Figure S8A,B). Notably, the temperature range (20−40 °C) in the experiment for the I−V characterization is above T_c. As the temperature increases, the interaction between PNRs is intensified and the average size of PNRs decreases, leading to a strength decrease of the spontaneous polarization.[46] The decrease of spontaneous polarization may result in the increase of the negative current if the negative current is suppressed by the spontaneous polarization.

However, we argue that reversible rectification does not originate mainly from the effect of spontaneous polarization mediated by the temperature, based on the following observations: (1) similar hysteresis characterization at positive bias is observed, which is independent of the temperature; (2) only negative current is largely changed by the temperature, while positive current remains almost unchanged. However, both positive and negative currents should be changed if the spontaneous polarization is largely influenced by the temperature. (3) The change of the rectification ratio strongly depends on the crystal size, which cannot be explained by the change of polarization mediated by the temperature.

To understand the underlying mechanism for the reversible rectification, we plot the energy landscape of the EGaIn−KTN−Au junction. The energy difference between the Fermi level and the valence band of KTN is determined to be 3.1 eV from the measurement of X-ray photoelectron spectroscopy (Figure S8). The Fermi level of KTN is determined to be −3.67 eV from the measurement of ultraviolet photoelectron spectroscopy (Figure S8). Therefore, the top of the valance band is calculated to be −6.77 eV. The band gap of KTN between the conduction band and the valence band is 3.6 eV,[38] and the Fermi level of EGaIn is −4.3 eV[25,47] and the Fermi level of gold is −5.1 eV according to the previous reports.[48,49] Taking this information, the energy landscape of the EGaIn−KTN−Au junction before contact can be figured out (Figure 3A). It is found that the Fermi levels of both the EGaIn and the Au electrodes are lower than the one of the KTN. Thus, Schottky contacts will be formed at the two terminal interfaces (EGaIn/KTN and KTN/Au) when the KTN is in contact with the electrodes (Figure 3B,C). Notably, the Schottky barrier at the KTN/Au interface is much higher than the one at the EGaIn/KTN interface, which turns out to be critical for the quasi-NDR observation.

Figure 3D,E shows the electron transfers at the two interfaces when a negative bias is applied on the EGaIn. The microscale crystals have higher surface defect density compared to a bulk crystal because additional defects (dislocations) may be introduced during grinding the bulk KTN crystal process, which leads to a poor integrity of the crystal surface.[50] Accordingly, the electrons may be trapped by the defects when the electrons reach the KTN/Au interface (Figure 3E). Thus, the current under negative bias will be suppressed. Notably, the trapping/detrapping events are strongly mediated by temperature, that is, less electrons are trapped by the defects when the temperature is increased due to the increased thermal energy of electrons, which makes it easier to escape from the trapping centers[51−53] (Figure 3I). Meanwhile, as the electrons transfer from the EGaIn to KTN, they will not be trapped regardless of the temperature due to the energy structure (Figure 3D,H). Taking two interfaces at

https://doi.org/10.1021/acsami.0c22925
ACS Appl. Mater. Interfaces 2021, 13, 29885−29893

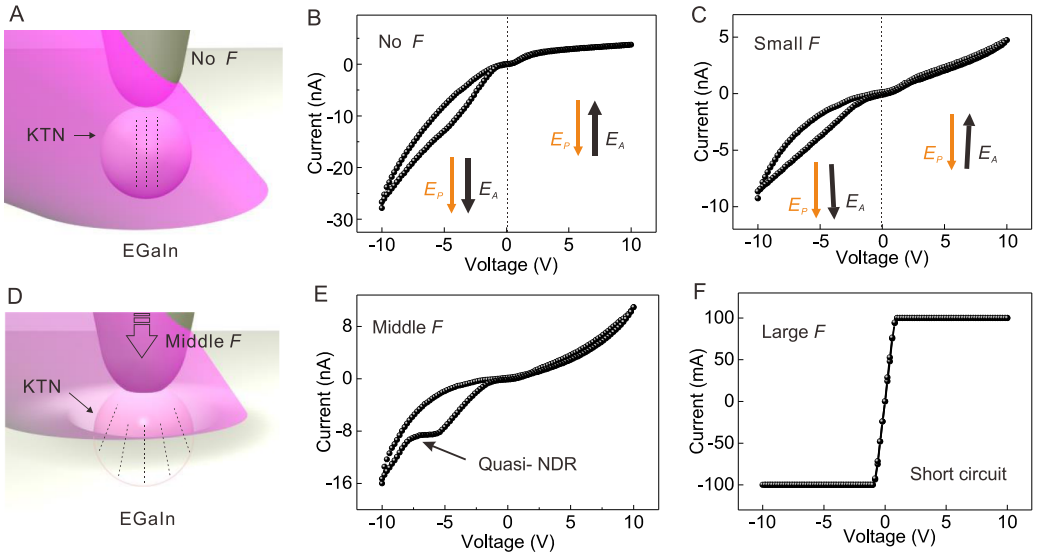

Figure 4. *I*–*V* curves of the EGaIn–KTN–EGaIn junction under different compression. (A) Schematic relative position of the top EGaIn electrode, KTN, and the bottom EGaIn electrode. The symbol ***F*** represents force exerted by the top electrode. Dashed lines indicate the transport path of the carriers. (B) *I*–*V* curve of the junction at the initial position without compression force. The black arrow indicates the applied electric field, $\boldsymbol{E}_{\mathbf{A}}$, and the red arrow indicates the spontaneous polarization, $\boldsymbol{E}_{\mathbf{P}}$. (C) *I*–*V* curve of the junction when compression force is increased. The relative direction between $\boldsymbol{E}_{\mathbf{A}}$ and $\boldsymbol{E}_{\mathbf{P}}$ is changed upon the compression. The direction of spontaneous polarization and applied electric field is not completely parallel/antiparallel. (D) Upon an increased compression force, an indentation appears on the surface of the bottom EGaIn electrode, which increases the contact area between KTN and the bottom EGaIn electrode. (E) Quasi-NDR is observed when the applied compression force is increased and the KTN is half-enclosed by the bottom EGaIn electrode. (F) Short circuit is observed upon a further hard compression.

the junction into consideration, the current under negative bias will increase due to the weakening of electron trapping of the defects when the temperature is increased. In contrast, the low Schottky barrier in the EGaIn/KTN interface can only trap few electrons when a positive bias is applied to the junction (Figure 3F). Therefore, the trapping events are only slightly influenced by the temperature (Figure 3J). For another interface of the junction, the electron will not be trapped regardless of the temperature as the electrons transfer from Au to KTN (Figure 3G,K). Therefore, the current can remain almost unchanged under positive bias.

Notably, the increase of temperature from 20 to 40° represents a small energy difference. While, we argue that such a small increase of the temperature can still lead to a large increase of the negative current. Based on the carrier trapping/detrapping model, we attribute it to the following factors: (1) the detrapping of carriers is enhanced by the increased temperature because the carriers can directly get additional energy from the environment as the temperature increases. This kinetic energy (the motion/mobility of carriers) will be enhanced under large bias voltage, which will in return assist the detrapping of carriers from the defect's states;[54] (2) the Femi level of KTN may be changed upon an increased temperature,[55] and the corresponding shifting of the energy alignment may lead to an easier detrapping of the carriers;[56] and (3) the trap density may degrade as the temperature is increased,[57] which will result in the increase of current upon increased temperature. Taking all the factors into consideration, the detrapping of carriers may be largely enhanced and the current under negative bias will increase when the temperature is increased.

Another possible mechanism for the observation of temperature-dependent rectification is that it originates from the effect of the oxide layer of the EGaIn electrode. Although the oxide layer is very thin, the oxide layer may influence the energy alignment, shifting the Fermi level of EGaIn lower with respect to KTN and thus preventing charge injection at negative bias, see Figure 3D. Another effect of the oxide layer is that the oxide layer could trap injected charges at negative bias. However, those trap states would lie above the Fermi level of pure EGaIn,[58] and thus charge trapping would rarely occur under positive bias. The oxide layer may be disrupted by thermal expansion and a small amount of liquid metal may exude from the electrode. The effect of the oxidation layer will be eliminated when the pure exuded EGaIn contacts directly with KTN, which will result in an increase of the current under negative bias as the temperature is increased. This mechanism can be employed to interpret the observation of temperature-dependent rectification ratio successfully, while it meets challenge to explain the electrode material-dependent rectification behavior, that is, the rectification is not influenced by the temperature as the Au electrode is replaced by graphene/Ag electrodes, see Supporting Information Figures S9 and S10. Also, it is difficult to explain quasi-NDR behavior using this model, see below.

Contact Geometry-Controlled Quasi-NDR. To fully understand the carrier transport through the microscale KTN, a symmetric EGaIn–KTN–EGaIn junction is fabricated by replacing the bottom Au electrode with another EGaIn electrode. Figure 4 shows the *I*–*V* curves of the symmetric junction upon laser (405 nm) illumination as the junction is compressed by raising the bottom EGaIn electrode at a fixed temperature (25 °C). With a close examination of Figure 4, two features can be observed: (1) the asymmetric *I*–*V* curves evolve to a symmetric one as the junction is compressed, see Figure 4B,E; (2) quasi-NDR is observed when an appropriate compression is applied and the crystals are half-enclosed by the bottom EGaIn electrode, see Figure 4E. We attribute the former observation to the change of the alignment between spontaneous polarization and applied electric field and

https://doi.org/10.1021/acsami.0c22925
ACS Appl. Mater. Interfaces 2021, 13, 29885–29893

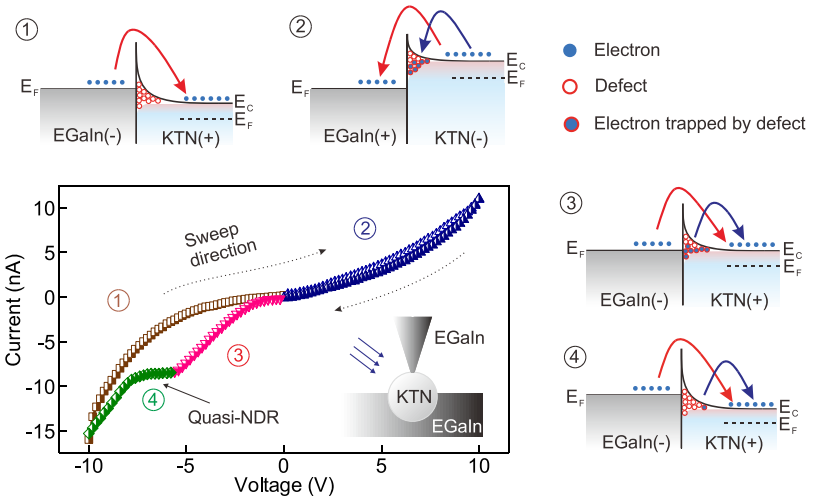

Figure 5. *I*−*V* curve and the mechanism for quasi-NDR in the EGaIn−KTN−EGaIn junction. The double sweep voltage starts from −10 V and ends at −10 V. The numbers indicate the sequence of the sweep process. The red arrows indicate the electron transport through the EGaIn−KTN interface driven by the applied bias. Blue arrows indicate the electron trapping/detrapping process due to the surface defects, which results in the observation of quasi-NDR. ①−④ Schematics of the electron transfer at the interface during the sweep process.

attribute the latter to the effect of additional surface defects introduced during the compression process, see below for details.

Because the bottom EGaIn electrode is a liquid-type metal, the bottom EGaIn surface will undergo a deformation upon compression, that is, the KTN particles may sink into the surface of the bottom EGaIn electrode, as schematically shown in Figure 4D. The applied electric field is along the vertical direction before the EGaIn deformation, as indicated by the dashed line in Figure 4A. When the KTN particle is half-enclosed by the EGaIn electrode, the applied electric field is directed upward from the bottom surface of the ball-shape KTN to the top EGaIn/KTN point contact, as indicated by the dashed line in Figure 4D. Depending on the detailed contact geometry (it is normally asymmetric along the central axis line between two electrodes), the paths of the carrier transport are redistributed as the junction is compressed, which will change the field alignment between spontaneous polarization and applied electric field.

The overall current will be suppressed when the applied electric field is antiparallel to the spontaneous polarization, refer to the positive current shown in Figure 4B. In contrast, the current will be enhanced when the applied electric field is parallel to the spontaneous polarization, see the negative current shown in Figure 4B. The effect of spontaneous polarization on current will be reduced when the applied field is not parallel to the spontaneous polarization (two arrows are tilted in Figure 4C), which will result in the increase of the positive current and the decrease of the negative current, as shown in Figure 4B,C.

Another interesting feature is that quasi-NDR behavior is observed, that is, the current of the junction does not increase as the bias voltage is negatively increased under a hard compression, as presented in Figures 4E and S11, S12. We attribute this quasi-NDR behavior to the effect of surface defects, which act as carrier trapping/detrapping centers. The defects should have more probability to be involved in the electric circuit when the junction is tightly compressed with the increasing contact area, thus the contact area will influence the carrier transport through the EGaIn−KTN−EGaIn junction.

Figure 5 shows the proposed mechanism for the quasi-NDR observation.[59] When a negative bias is applied to the bottom EGaIn electrode, the carriers overcome the Schottky barrier to form a current (I_{driven}), as indicated by the red arrow in the process ①. In this process, the surface defects do not affect the carrier transport. However, the surface defects strongly influence the carrier transport when the electron transfers across the KTN/EGaIn interface as a positive bias is applied, see process ②. In this process, the electrons will be partially trapped by the surface defects, and parts of the electron can pass through the barrier, as indicated by the red arrow. Therefore, the current is suppressed under positive bias voltage until all the trapping states are filled by the carriers,[60] resulting in a smaller current compared to the one under the negative bias.

When a reversed voltage sweep is applied, the trapped electrons will be released gradually from the trapping centers resulting an additional current ($I_{release}$), see process ③. Correspondingly, the current increases considerably due to the contribution by both I_{driven} and $I_{release}$, as indicated by the red arrow and blue arrow in process ③. With a close examination of process ③, it can be found that the current is quite small at the beginning of process ③, which is attributed to the fact that the barrier for electron injection is high due to the trapped electrons under positive bias (process ②). When the electrons begin to be detrapped, a reduced barrier occurs. The reduced barrier together with the detrapped electron will result in the fast increase of the current, see the end part of ③.

When the detrapped electron is reduced, the fast increase of current cannot be sustained any more, which results in a gradual decrease of the current (quasi-NDR), see the beginning part of process ④. When all the trapped electrons are detrapped, the barrier for the electron injection is further reduced, which results in a fast increase of current once more, see the end part of process ④. Contrary to expectation, the quasi-NDR is only observed under negative bias and no quasi-NDR is observed under positive bias in the symmetric EGaIn−KTN−EGaIn junction. We attribute it to the asymmetric contact geometry, that is, the microscale KTN is in point contact with the top EGaIn electrode but is in surface contact with the bottom EGaIn electrode in which the considerable

https://doi.org/10.1021/acsami.0c22925
ACS Appl. Mater. Interfaces 2021, 13, 29885−29893

surface defects will play an import role in determining the carrier transport through the microscale KTN. The force-controlled quasi-NDR behavior has a potential application in force-related sensor and functional nanoelectronic circuits.

CONCLUSIONS

In summary, a method exploiting liquid metal (EGaIn) as a top electrode is developed to study the properties of microscale KTN crystal particles. The EGaIn can be used as a "print ink" to produce electric circuits directly, and has wide potential application in flexible electronic circuits. Unlike the bulk crystals, the surface defects play a critical role in determining the carrier transport through the microscale KTN junction. The current under negative bias can be enhanced by two orders of magnitude, but the current under positive bias remains unchanged when the temperature is increased by 20 °C, which results in a reversible rectification. Additionally, a quasi-NDR is observed in the symmetric EGaIn−KTN−EGaIn junctions by the control of the contact geometry. The underlying mechanism for these observations is proposed based on the measured energy landscape, that is, the carrier trapping/detrapping determined by the energy structure of the junction strongly depends on the ambient temperature and contact geometry. Our results will assist in understanding the carrier conduction in microscale ferroelectric materials upon light illumination, assisting to fabricate a switchable diode via temperature control and contact area-mediated quasi-NDR devices via force control.

EXPERIMENTAL SECTION

Preparation of Microscale KTN Crystals. The original bulk KTN crystal is ordered from NTT Advanced Technology Corporation. The KTN is ground into small particles in an agate mortar with alcohol used as a dispersant. The KTN particles are then put into an ultrasonic cleaning apparatus for dispersion. The dispersed solvent is dropped on the clean Au bottom surface. The KTN crystals with an appropriate size (50−200 μm in length) are picked up for further investigation after the evaporation of ethanol in a vacuum chamber at room temperature.

Photocurrent Measurements. The position and movement of the bottom Au electrode is controlled using PiezoWalk actuators (PI, N-111, Germany), which can move continuously in the vertical direction with a resolution of 0.1 nm and a maximum travel range of 10 mm. The light power is measured using a light power meter (Thorlabs PM400D). The Daheng Optics' GCI-73M electronic timer and series shutters are used to control the duration of light illumination. The real-time current response upon light irradiation is recorded using a semiconductor analyzer (B1500A, KEYSIGHT).

ASSOCIATED CONTENT

Supporting Information

The Supporting Information is available free of charge at https://pubs.acs.org/doi/10.1021/acsami.0c22925.

Photographs of KTN with different sizes; procedure for the fabrication of EGaIn tips; EGaIn−KTN−Au junction formation and separation process; measurement system and photocurrent response of the KTN junction; $I-V$ curves of the microscale KTN particles and bulk KTN cube under light illumination; and characterization and energy structure of KTN crystals (PDF)

Fabrication of an EGaIn conical tip (MP4)

Formation of the EGaIn−KTN−Au junction (MP4)

AUTHOR INFORMATION

Corresponding Authors

Takhee Lee − *Department of Physics and Astronomy, and Institute of Applied Physics, Seoul National University, Seoul 08826, Korea;* orcid.org/0000-0001-5988-5219; Phone: 0082-2-880-4269; Email: tlee@snu.ac.kr

Hongliang Liu − *Tianjin Key Laboratory of Micro-scale Optical Information Science and Technology, Institute of Modern Optics, Nankai University, Tianjin 300350, China; State Key Laboratory of Crystal Materials, Shandong University, Jinan 250100, China;* orcid.org/0000-0003-0792-4284; Phone: 0086-130-7229-2263; Email: drliuhl@nankai.edu.cn

Dong Xiang − *Tianjin Key Laboratory of Micro-scale Optical Information Science and Technology, Institute of Modern Optics, Nankai University, Tianjin 300350, China; Center of Single Molecule Sciences, College of Electronic Information and Optical Engineering, Nankai University, Tianjin 300350, China;* orcid.org/0000-0002-5632-6355; Phone: 0086-151-0224-4129; Email: xiangdongde@nankai.edu.cn

Authors

Lifa Ni − *Tianjin Key Laboratory of Micro-scale Optical Information Science and Technology, Institute of Modern Optics, Nankai University, Tianjin 300350, China; Center of Single Molecule Sciences, College of Electronic Information and Optical Engineering, Nankai University, Tianjin 300350, China*

Xiaojin Li − *Tianjin Key Laboratory of Micro-scale Optical Information Science and Technology, Institute of Modern Optics, Nankai University, Tianjin 300350, China*

Zhibin Zhao − *Tianjin Key Laboratory of Micro-scale Optical Information Science and Technology, Institute of Modern Optics, Nankai University, Tianjin 300350, China; Center of Single Molecule Sciences, College of Electronic Information and Optical Engineering, Nankai University, Tianjin 300350, China*

Jongwoo Nam − *Department of Physics and Astronomy, and Institute of Applied Physics, Seoul National University, Seoul 08826, Korea*

Pengfei Wu − *Tianjin Key Laboratory of Micro-scale Optical Information Science and Technology, Institute of Modern Optics, Nankai University, Tianjin 300350, China*

Qingling Wang − *Tianjin Key Laboratory of Micro-scale Optical Information Science and Technology, Institute of Modern Optics, Nankai University, Tianjin 300350, China*

Complete contact information is available at: https://pubs.acs.org/10.1021/acsami.0c22925

Author Contributions

The manuscript was written through contributions of all authors. All authors have given approval to the final version of the manuscript. L. N. and X. L. contributed equally.

Notes

The authors declare no competing financial interest.

ACKNOWLEDGMENTS

We acknowledge the financial support from the National Natural Science Foundation of China (91950116, 61571242, 11804170, and 11704201) and Natural Science Foundation of Tianjin City (19JCZDJC31000 and 19JCJQJC60900). J.N. and T. L. appreciate the financial support of the National

Research Foundation grant (No. 2021R1A2C3004783) by the Ministry of Science and ICT of Korea.

■ ABBREVIATIONS

KTN, potassium tantalate niobate
EGaIn, eutectic gallium indium
NDR, negative differential resistance.

■ REFERENCES

(1) Berdan, R.; Marukame, T.; Ota, K.; Yamaguchi, M.; Saitoh, M.; Fujii, S.; Deguchi, J.; Nishi, Y. Low-Power Linear Computation Using Nonlinear Ferroelectric Tunnel Junction Memristors. *Nat. Electron.* **2020**, *3*, 259−266.

(2) Ma, C.; Luo, Z.; Huang, W.; Zhao, L.; Chen, Q.; Lin, Y.; Liu, X.; Chen, Z.; Liu, C.; Sun, H.; Jin, X.; Yin, Y.; Li, X. Sub-Nanosecond Memristor Based on Ferroelectric Tunnel Junction. *Nat. Commun.* **2020**, *11*, 1439.

(3) Wu, G.; Tian, B.; Liu, L.; Lv, W.; Wu, S.; Wang, X.; Chen, Y.; Li, J.; Wang, Z.; Wu, S.; Shen, H.; Lin, T.; Zhou, P.; Liu, Q.; Duan, C.; Zhang, S.; Meng, X.; Wu, S.; Hu, W.; Wang, X.; Chu, J.; Wang, J. Programmable Transition Metal Dichalcogenide Homojunctions Controlled by Nonvolatile Ferroelectric Domains. *Nat. Electron.* **2020**, *3*, 43−50.

(4) Wen, Z.; Wu, D. Ferroelectric Tunnel Junctions: Modulations on the Potential Barrier. *Adv. Mater.* **2020**, *32*, 1904123.

(5) Wang, X.; Wang, J. Ferroelectric Tunnel Junctions with High Tunnelling Electroresistance. *Nat. Electron.* **2020**, *3*, 440−441.

(6) Choi, T.; Lee, S.; Choi, Y. J.; Kiryukhin, V.; Cheong, S.-W. Switchable Ferroelectric Diode and Photovoltaic Effect in $BiFeO_3$. *Science* **2009**, *324*, 63−66.

(7) Yin, L.; Mi, W. Progress in $BiFeO_3$-Based Heterostructures: Materials, Properties and Applications. *Nanoscale* **2020**, *12*, 477−523.

(8) Shinagawa, M.; Kobayashi, J.; Yagi, S.; Sakai, Y. Sensitive Electro-Optic Sensor Using $KTa_{1-x}Nb_xO_3$ Crystal. *Sens. Actuators, A* **2013**, *192*, 42−48.

(9) Zhu, W.; Chao, J.-H.; Chen, C.-J.; Shang, A.; Lee, Y. G.; Yin, S.; Dubinskii, M.; Hoffman, R. C. Photon Excitation Enabled Large Aperture Space-Charge-Controlled Potassium Tantalate Niobate (KTN) Beam Deflector. *Appl. Phys. Lett.* **2018**, *112*, 132901.

(10) Szabados, J.; Werner, C. S.; Herr, S. J.; Breunig, I.; Buse, K. Electro-Optic Eigenfrequency Tuning of Potassium Tantalate-Niobate Microresonators. *APL Photonics* **2020**, *5*, 016106.

(11) Fu, H.; Cohen, R. E. Polarization Rotation Mechanism for Ultrahigh Electromechanical Response in Single-Crystal Piezoelectrics. *Nature* **2000**, *403*, 281−283.

(12) Ren, X. Large Electric-Field-Induced Strain in Ferroelectric Crystals by Point-Defect-Mediated Reversible Domain Switching. *Nat. Mater.* **2004**, *3*, 91−94.

(13) DelRe, E.; Spinozzi, E.; Agranat, A. J.; Conti, C. Scale-Free Optics and Diffractionless Waves in Nanodisordered Ferroelectrics. *Nat. Photonics* **2011**, *5*, 39−42.

(14) Li, J.; Li, Y.; Meng, Q.; Zhou, Z.; Jia, D.; McIntosh, R.; Bhalla, A. S.; Guo, R. Large Electro-Optic Response of Bulk Ferroelectric Crystals Enhanced by Piezoelectric Resonance in the High Frequency Range. *Mater. Res. Bull.* **2018**, *97*, 523−529.

(15) Huang, F.; Tian, H.; Meng, X.; Tan, P.; Cao, X.; Bai, Y.; Hu, C.; Zhou, Z. Large Room Temperature Electrocaloric Effect in $KTa_{1-x}Nb_xO_3$ Single Crystal. *Phys. Status Solidi RRL* **2019**, *13*, 1800515.

(16) Grabecki, G.; Dabrowski, A.; Iwanowski, P.; Hruban, A.; Kowalski, B. J.; Olszowska, N.; Kolodziej, J.; Chojnacki, M.; Dybko, K.; Lusakowski, A.; Wojtowicz, T.; Wojciechowski, T.; Jakiela, R.; Wisniewski, A. Conductance Spectra of (Nb, Pb, In)/NbP Superconductor/Weyl Semimetal Junctions. *Phys. Rev. B* **2020**, *101*, 085113.

(17) Bonkerud, J.; Zimmermann, C.; Weiser, P. M.; Aarholt, T.; Verhoeven, E. F.; Vines, L.; Monakhov, E. V.; Herklotz, F. Fabrication and Characterization of Schottky Barrier Diodes on Rutile TiO_2. *Mater. Res. Express* **2020**, *7*, 065903.

(18) Simeone, F. C.; Yoon, H. J.; Thuo, M. M.; Barber, J. R.; Smith, B.; Whitesides, G. M. Defining the Value of Injection Current and Effective Electrical Contact Area for EGaIn-Based Molecular Tunneling Junctions. *J. Am. Chem. Soc.* **2013**, *135*, 18131−18144.

(19) Thuo, M. M.; Reus, W. F.; Simeone, F. C.; Kim, C.; Schulz, M. D.; Yoon, H. J.; Whitesides, G. M. Replacing $-CH_2CH_2-$ with $-CONH-$ Does Not Significantly Change Rates of Charge Transport through Ag^{TS}-SAM//Ga_2O_3/EGaIn Junctions. *J. Am. Chem. Soc.* **2012**, *134*, 10876−10884.

(20) Liao, K.-C.; Yoon, H. J.; Bowers, C. M.; Simeone, F. C.; Whitesides, G. M. Replacing $Ag^{TS}SCH_2$-R with $Ag^{TS}O_2C$-R in EGaIn-Based Tunneling Junctions Does Not Significantly Change Rates of Charge Transport. *Angew. Chem., Int. Ed.* **2014**, *53*, 3889−3893.

(21) Nijhuis, C. A.; Reus, W. F.; Whitesides, G. M. Molecular Rectification in Metal-SAM-Metal Oxide-Metal Junctions. *J. Am. Chem. Soc.* **2009**, *131*, 17814−17827.

(22) Chiechi, R. C.; Weiss, E. A.; Dickey, M. D.; Whitesides, G. M. Eutectic Gallium-Indium (EGaIn): A Moldable Liquid Metal for Electrical Characterization of Self-Assembled Monolayers. *Angew. Chem., Int. Ed.* **2008**, *47*, 142−144.

(23) Fracasso, D.; Muglali, M. I.; Rohwerder, M.; Terfort, A.; Chiechi, R. C. Influence of an Atom in EGaIn/Ga_2O_3 Tunneling Junctions Comprising Self-Assembled Monolayers. *J. Phys. Chem. C* **2013**, *117*, 11367−11376.

(24) Wan, A.; Jiang, L.; Sangeeth, C. S. S.; Nijhuis, C. A. Reversible Soft Top-Contacts to Yield Molecular Junctions with Precise and Reproducible Electrical Characteristics. *Adv. Funct. Mater.* **2014**, *24*, 4442−4456.

(25) Nerngchamnong, N.; Yuan, L.; Qi, D.-C.; Li, J.; Thompson, D.; Nijhuis, C. A. The Role of Van Der Waals Forces in the Performance of Molecular Diodes. *Nat. Nanotechnol.* **2013**, *8*, 113−118.

(26) Zhao, Z.; Wang, W.; Zhou, X.; Ni, L.; Kang, K.; Lee, T.; Han, H.; Yuan, H.; Guo, C.; Wang, M.; Ko, M. J.; Li, Y.; Xiang, D. Crystal Size Effect on Carrier Transport of Microscale Perovskite Junctions via Soft Contact. *Nano Lett.* **2020**, *20*, 8640−8646.

(27) Díez-Pérez, I.; Hihath, J.; Lee, Y.; Yu, L.; Adamska, L.; Kozhushner, M. A.; Oleynik, I. I.; Tao, N. Rectification and Stability of a Single Molecular Diode with Controlled Orientation. *Nat. Chem.* **2009**, *1*, 635−641.

(28) Di Bartolomeo, A. Graphene Schottky Diodes: An Experimental Review of the Rectifying Graphene/Semiconductor Heterojunction. *Phys. Rep.* **2016**, *606*, 1−58.

(29) Capozzi, B.; Xia, J.; Adak, O.; Dell, E. J.; Liu, Z.-F.; Taylor, J. C.; Neaton, J. B.; Campos, L. M.; Venkataraman, L. Single-Molecule Diodes with High Rectification Ratios through Environmental Control. *Nat. Nanotechnol.* **2015**, *10*, 522−527.

(30) Yang, G.; Jia, C. H.; Chen, Y. H.; Chen, X.; Zhang, W. F. Negative Differential Resistance and Resistance Switching Behaviors in $BaTiO_3$ Thin Films. *J. Appl. Phys.* **2014**, *115*, 204515.

(31) Tuomisto, N.; van Dijken, S.; Puska, M. Tsu-Esaki Modeling of Tunneling Currents in Ferroelectric Tunnel Junctions. *J. Appl. Phys.* **2017**, *122*, 234301.

(32) Zhao, P.; Cui, H. L.; Woolard, D.; Jensen, K. L.; Buot, F. A. Simulation of Resonant Tunneling Structures: Origin of the I-V Hysteresis and Plateau-Like Structure. *J. Appl. Phys.* **2000**, *87*, 1337−1349.

(33) Broekaert, T. P. E.; Brar, B.; van der Wagt, J. P. A.; Seabaugh, A. C.; Morris, F. J.; Moise, T. S.; Beam, E. A.; Frazier, G. A. A Monolithic 4-bit 2-Gsps Resonant Tunneling Analog-to-Digital Converter. *IEEE J. Solid State Circ.* **1998**, *33*, 1342−1349.

(34) Mathews, R. H.; Sage, J. P.; Sollner, T. C. L. G.; Calawa, S. D.; Chen, C.-L.; Mahoney, L. J.; Maki, P. A.; Molvar, K. M. A New RTD-FET Logic Family. *Proc. IEEE* **1999**, *87*, 596−605.

(35) Suzuki, S.; Asada, M.; Teranishi, A.; Sugiyama, H.; Yokoyama, H. Fundamental Oscillation of Resonant Tunneling Diodes Above 1 THz at Room Temperature. *Appl. Phys. Lett.* **2010**, *97*, 242102.

https://doi.org/10.1021/acsami.0c22925
ACS Appl. Mater. Interfaces 2021, 13, 29885−29893

(36) Reddy, M.; Martin, S. C.; Molnar, A. C.; Muller, R. E.; Smith, R. P.; Siegel, P. H.; Mondry, M. J.; Rodwell, M. J. W.; Kroemer, H.; Allen, S. J. Monolithic Schottky-Collector Resonant Tunnel Diode Oscillator Arrays to 650 GHz. *IEEE Electron Device Lett.* **1997**, *18*, 218−221.
(37) Chen, X.; Hu, H.; Trasobares, J.; Nijhuis, C. A. Rectification Ratio and Tunneling Decay Coefficient Depend on the Contact Geometry Revealed by in Situ Imaging of the Formation of EGaIn Junctions. *ACS Appl. Mater. Interfaces* **2019**, *11*, 21018−21029.
(38) Didomenico, M.; Wemple, S. H. Optical Properties of Perovskite Oxides in Their Paraelectric and Ferroelectric Phases. *Phys. Rev.* **1968**, *166*, 565−576.
(39) Han, Q.; Bae, S. H.; Sun, P.; Hsieh, Y. T.; Yang, Y.; Rim, Y. S.; Zhao, H.; Chen, Q.; Shi, W.; Li, G.; Yang, Y. Single Crystal Formamidinium Lead Iodide ($FAPbI_3$): Insight into the Structural, Optical, and Electrical Properties. *Adv. Mater.* **2016**, *28*, 2253−2258.
(40) Cui, X.; Yuan, S.; Zhang, H.; Zhang, X.; Wang, P.; Tu, L.; Sun, Z.; Wang, J.; Zhan, Y.; Zheng, L. Temperature-Dependent Electronic Properties of Inorganic-Organic Hybrid Halide Perovskite ($CH_3NH_3PbBr_3$) Single Crystal. *Appl. Phys. Lett.* **2017**, *111*, 233302.
(41) Jeong, H. J.; Bang, S.; Park, D. Y.; Jeon, H.; Namkoong, G.; Jeong, M. S. Fabrication of Pyramidal (111) $MAPbBr_3$ Film with Low Surface Defect Density Using Homogeneous Quantum-Dot Seeds. *Nanoscale* **2020**, *12*, 1366−1373.
(42) Stranks, S. D.; Eperon, G. E.; Grancini, G.; Menelaou, C.; Alcocer, M. J. P.; Leijtens, T.; Herz, L. M.; Petrozza, A.; Snaith, H. J. Electron-Hole Diffusion Lengths Exceeding 1 Micrometer in an Organometal Trihalide Perovskite Absorber. *Science* **2013**, *342*, 341−344.
(43) Dong, Q.; Fang, Y.; Shao, Y.; Mulligan, P.; Qiu, J.; Cao, L.; Huang, J. Electron-hole diffusion lengths > 175 μm in Solution-Grown $CH_3NH_3PbI_3$ Single Crystals. *Science* **2015**, *347*, 967−970.
(44) Chen, J.; You, D.; Zhang, Y.; Zhang, T.; Yao, C.; Zhang, Q.; Li, M.; Lu, Y.; He, Y. Highly Sensitive and Tunable Self-Powered UV Photodetectors Driven Jointly by p-n Junction and Ferroelectric Polarization. *ACS Appl. Mater. Interfaces* **2020**, *12*, 53957−53965.
(45) Eremenko, M.; Krayzman, V.; Bosak, A.; Playford, H. Y.; Chapman, K. W.; Woicik, J. C.; Ravel, B.; Levin, I. Local Atomic Order and Hierarchical Polar Nanoregions in a Classical Relaxor Ferroelectric. *Nat. Commun.* **2019**, *10*, 2728.
(46) Li, X.; Yang, Q.; Zhang, X.; He, S.; Liu, H.; Wu, P. Heating-Rate-Dependent Dielectric Properties of $KTa_{0.58}Nb_{0.42}O_3$ Crystal in Paraelectric Phase. *Cryst. Growth Des.* **2020**, *20*, 2578−2583.
(47) Sangeeth, C. S. S.; Demissie, A. T.; Yuan, L.; Wang, T.; Frisbie, C. D.; Nijhuis, C. A. Comparison of DC and AC Transport in 1.5-7.5 nm Oligophenylene (mine Molecular Wires across Two Junction Platforms: Eutectic Ga-In versus Conducting Probe Atomic Force Microscope Junctions. *J. Am. Chem. Soc.* **2016**, *138*, 7305−7314.
(48) Nijhuis, C. A.; Reus, W. F.; Barber, J. R.; Dickey, M. D.; Whitesides, G. M. Charge Transport and Rectification in Arrays of SAM-based Tunneling Junctions. *Nano Lett.* **2010**, *10*, 3611−3619.
(49) Nijhuis, C. A.; Reus, W. F.; Whitesides, G. M. Mechanism of Rectification in Tunneling Junctions Based on Molecules with Asymmetric Potential Drops. *J. Am. Chem. Soc.* **2010**, *132*, 18386−18401.
(50) Oh, E.; Gye, G.; Yeom, H. W. Defect-Selective Charge-Density-Wave Condensation in 2H-NbSe_{2}. *Phys. Rev. Lett.* **2020**, *125*, 036804.
(51) Lee, M.; Ahn, C. W.; Vu, T. K. O.; Lee, H. U.; Jeong, Y.; Hahm, M. G.; Kim, E. K.; Park, S. Current Transport Mechanism in Palladium Schottky Contact on Si-Based Freestanding GaN. *Nanomaterials* **2020**, *10*, 297.
(52) Liu, N.; Liu, P.; Zhou, H.; Bai, Y.; Chen, Q. Understanding the Defect Properties of Quasi-2D Halide Perovskites for Photovoltaic Applications. *J. Phys. Chem. Lett.* **2020**, *11*, 3521−3528.
(53) Islam, M. M.; Adhikari, N.; Hernandez, A.; Janover, A.; Novak, S.; Agarwal, S.; Codding, C. L.; Snure, M.; Huang, M.; Selim, F. A. Direct Measurement of the Density and Energy Level of Compensating Acceptors and Their Impact on the Conductivity of N-Type Ga_2O_3 Films. *J. Appl. Phys.* **2020**, *127*, 145701.
(54) Haneef, H. F.; Zeidell, A. M.; Jurchescu, O. D. Charge Carrier Traps in Organic Semiconductors: A Review on the Underlying Physics and Impact on Electronic Devices. *J. Mater. Chem. C* **2020**, *8*, 759−787.
(55) Nguyen, T. H.; O'Leary, S. K. The Dependence of the Fermi Level on Temperature, Doping Concentration, and Disorder in Disordered Semiconductors. *J. Appl. Phys.* **2000**, *88*, 3479−3483.
(56) Maeda, T.; Okada, M.; Ueno, M.; Yamamoto, Y.; Kimoto, T.; Horita, M.; Suda, J. Temperature Dependence of Barrier Height in Ni/n-GaN Schottky Barrier Diode. *Appl. Phys. Express* **2017**, *10*, 051002.
(57) Sun, C.; Liang, R.; Xiao, L.; Liu, L.; Xu, J.; Wang, J. Effect of Traps and Defects on High Temperature Performance of Ge Channel Junctionless Nanowire Transistors. *AIP Adv.* **2017**, *7*, 075009.
(58) Wimbush, K. S.; Fratila, R. M.; Wang, D.; Qi, D.; Liang, C.; Yuan, L.; Yakovlev, N.; Loh, K. P.; Reinhoudt, D. N.; Velders, A. H.; Nijhuis, C. A. Bias Induced Transition from an Ohmic to a Non-Ohmic Interface in Supramolecular Tunneling Junctions with Ga_2O_3/EGaIn Top Electrodes. *Nanoscale* **2014**, *6*, 11246−11258.
(59) He, J.; Zhu, J.; Ma, C.; Lu, J.; Hu, Z. Negative Differential Resistance and Multilevel Resistive Switching in $BaSrTiO_3$ Films. *Appl. Phys. Lett.* **2019**, *115*, 072101.
(60) Liu, Y.; Sun, J.; Yang, Z.; Yang, D.; Ren, X.; Xu, H.; Yang, Z.; Liu, S. F. 20-mm-Large Single-Crystalline Formamidinium-Perovskite Wafer for Mass Production of Integrated Photodetectors. *Adv. Mater. Opt. Electron.* **2016**, *4*, 1829−1837.

https://doi.org/10.1021/acsami.0c22925
ACS Appl. Mater. Interfaces 2021, 13, 29885−29893